FUNCTIONAL SUBCLONE PROFILING FOR PREDICTION OF TREATMENT-INDUCED INTRA-TUMOR POPULATION SHIFTS AND DISCOVERY OF RATIONAL DRUG COMBINATIONS IN HUMAN GLIOBLASTOMA

Roman Reinartz[1,2], **Shanshan Wang**[3], **Sied Kebir**[1,2], **Daniel J. Silver**[4], **Anja Wieland**[1,2], **Tong Zheng**[3], **Marius Küpper**[1,2], **Laurèl Rauschenbach**[1,2], **Rolf Fimmers**[5], **Timothy M. Shepherd**[6], **Daniel Trageser**[1,2,7], **Andreas Till**[1,2], **Niklas Schäfer**[1,2], **Martin Glas**[1,2,7], **Axel M. Hillmer**[8], **Sven Cichon**[9], **Amy A. Smith**[10], **Torsten Pietsch**[11], **Ying Liu**[12], **Brent A. Reynolds**[3], **Anthony Yachnis**[13], **David W. Pincus**[3], **Matthias Simon**[14], **Oliver Brüstle**[2,7,15], **Dennis A. Steindler**[16,*], and **Björn Scheffler**[1,2,7,17, ,*]

[1]Stem Cell Pathologies, University Bonn Med Ctr, 53105 Bonn, Germany [2]Inst Reconstructive Neurobiology, University Bonn Med Ctr, 53105 Bonn, Germany [3]Dept Neurosurgery, University of Florida, Gainesville, FL 32611, USA [4]Dept Cellular & Molecular Medicine, Cleveland Clinic Lerner Res Inst, OH 44195, USA [5]Inst for Medical Biometry, Informatics & Epidemiology, University of Bonn, 53105 Bonn, Germany [6]Dept Neuroradiology, NYU Langone Medical Center, NY 10016, USA [7]LIFE & BRAIN GmbH, 53105 Bonn, Germany [8]Cancer Therapeutics and Stratified Oncology, Genome Institute of Singapore, 138672 Singapore [9]Division of Medical Genetics, University of Basel, 4031 Basel, Switzerland [10]University of Florida, Health Cancer Center at Orlando Health, FL 32806, USA [11]Dept of Neuropathology, University Bonn Med Ctr, 53015 Bonn, Germany [12]Dept of Neurosurgery and Ctr for Stem Cell & Regen Medicine, The Brown Foundation Institute of Molecular Medicine, The University of Texas Health Science Center at Houston, TX 77030, USA [13]Dept of Pathology, Immunology, & Lab Medicine, University of Florida,

To whom correspondence may be addressed: Björn Scheffler, M.D., Institute of Reconstructive Neurobiology / Life & Brain Ctr, University of Bonn Medical Ctr., Sigmund Freud Str. 25, D-53105 Bonn, Germany, Tel: (+) 49-228-6885-473, Fax: (+) 49-228-6885-443, bscheffler@uni-bonn.de.
*shared last authors

The authors declare no conflict of interests

AUTHOR CONTRIBUTIONS

COMPETING FINANCIAL INTEREST

The authors declare no competing financial interests.

Gainesville, FL 32603, USA [14]Clinic for Neurosurgery, University Bonn Med Ctr, 53105 Bonn, Germany [15]DZNE – German Center for Neurodegenerative Disease, 53105 Bonn, Germany [16]JM USDA Human Nutrition Research Center on Aging, Tufts University, Boston, MA 02111, USA [17]DKFZ-Division of Translational Oncology / Neurooncology, German Cancer Consortium (DKTK), Heidelberg & University Hospital Essen, 45147 Essen, Germany

Abstract

Purpose—Investigation of clonal heterogeneity may be key to understanding mechanisms of therapeutic failure in human cancer. However, little is known on the consequences of therapeutic intervention on the clonal composition of solid tumors.

Experimental Design—Here, we used 33 single cell-derived subclones generated from five clinical glioblastoma specimens for exploring intra- and inter-individual spectra of drug resistance profiles *in vitro*. In a personalized setting, we explored whether differences in pharmacological sensitivity among subclones could be employed to predict drug-dependent changes to the clonal composition of tumors.

Results—Subclones from individual tumors exhibited a remarkable heterogeneity of drug resistance to a library of potential anti-glioblastoma compounds. A more comprehensive intra-tumoral analysis revealed that stable genetic and phenotypic characteristics of co-existing subclones could be correlated with distinct drug sensitivity profiles. The data obtained from differential drug response analysis could be employed to predict clonal population shifts within the naïve parental tumor *in vitro* and in orthotopic xenografts. Furthermore, the value of pharmacological profiles could be shown for establishing rational strategies for individualized secondary lines of treatment.

Conclusions—Our data provide a previously unrecognized strategy for revealing functional consequences of intra-tumor heterogeneity by enabling predictive modeling of treatment-related subclone dynamics in human glioblastoma.

Keywords

INTRODUCTION

Cellular heterogeneity has traditionally been viewed as a result of hyperproliferation and increasing genetic instability that at late stages of tumor progression leads to the spawning of subclones (1, 2). Their phylogeny can be recapitulated, e.g. by applying single nucleus deep sequencing, regional dissections, or visualization of specific genetic hallmarks (3–5). On a practical note, increasing degrees of intra-tumor heterogeneity are acknowledged as an indicator for unfavorable disease progression/prognosis (6–8) and it is thought that heterogeneity data could have the potential to influence clinical decision-making (9). But this is not routinely applied in the field yet. One aspect is a lack of preclinical model systems that could help to better understand the impact of chemotherapy on clonal heterogeneity.

Ideal models would have to implement genetic/phenotypic identity of subclones with the respective cellular function for monitoring drug effects over time in a given tumor (10).

In many of the particularly malignant cancers, e.g. the primary brain tumor glioblastoma, (stem-like) subclones with intrinsic drug resistances are considered to account for treatment failure and relapse that inevitably occur during the course of disease (11–13). Recent insights from *in vitro* studies on intra-individual drug response suggest that subclones with differential resistance profiles co-exist in glioblastoma (14). Here, we found that single cell-derived subclones of clinical glioblastoma samples maintain their distinct phenotypic and genetic identities *ex vivo* and that their pharmacological profiles enable experimental access to model specific subclone targeting *in vitro* and *in vivo*. As a consequence, drug-related polyclonal population dynamics becomes predictable. A major further benefit of this approach is the previously unrecognized feature to identify subclone-specific drug combinations suited for sequential targeting of co-existing tumor cell hierarchies, which reflect the foundation of intra-tumor heterogeneity.

MATERIALS AND METHODS

Tissue Samples

Tumor tissue was obtained from glioblastoma surgery at the University of Bonn (BN035-BN118, Bonn, Germany) and the University of Florida (GNV019, Gainesville, FL, USA, patient details: Supplementary Table S1). Local ethics committees at both sites approved the studies, and patients or their guardians provided informed consent. Tissue diagnosis/grading based on the WHO classification (15, 16).

Tissue handling and cell culture

Handling of tissue and cell-derivation protocols (BN035-BN118/GNV019) were described (17, 18). Samples were analyzed at *in vitro* passages 5–13. Subclones derived from passage 5/6 parental cells and were investigated at subsequent *in vitro* passages 2–8. With exception of the neurosphere assay and the extreme limiting dilution assay (ELDA), samples were grown adherently on laminin (Life Technologies) /poly-L-ornithine (Sigma-Aldrich)-coated (PO) plasticware (17, 18). Culture methods for reference/control cells were described: U87(MG) glioma cell line, hnNCs (human non-malignant neural cells: short-term expanded hippocampus-derived adult human neural progenitors) (18), and hESCdNPs (human ES cell-derived neural progenitor cells; 19). Cell line authentication was conducted by the DSMZ (Braunschweig, Germany) using STR analysis, last tested in September 2015 (U87(MG)). Human primary fibroblasts (FIBRO) were provided by Dr. Phillip Koch and expanded in DMEM/F12 media (Life Technologies) supplemented with 10% fetal calf serum (Hyclone, GE Healthcare) and 1% antibiotic-antimycotic. All investigated cells tested mycoplasm-negative per standard cell-lysate PCR detection. For *in vitro* growth kinetics, populations doublings (PD) were calculated: n=3.32(log UCY − log l)+X, where (n)=final PD number at end of given subculture; (UCY)=cell yield at that point; (I)=cell number used as inoculum of subculture; (X)=doubling level of inoculum used to initiate the quantified subculture. The neurosphere assay testing cellular differentiation was applied as described (17, 20). For the ELDA, GNV019 cells plated in a volume of 150 μl on ultra low attachment 96-well plates

(Corning) in decreasing numbers for 7 days were incubated with Calcein AM viability dye (5 μM) for 30 min to label vital cells and for fluorescence-based quantification of tumor spheres.

Derivation of tumor subclones

Passage 5 GNV019 cells were plated at 15 cells/cm^2 on five PO-coated 10 cm dishes. 20 individual cells/dish were randomly selected on the subsequent day, marked with pen at bottom of dish, and followed for 30–60 days. Seven of these formed clonal colonies, were selected using 8 mm cloning cylinders (Corning), trypsinized, and transferred to a 6 cm dish for expansion. CL1/2/3/6/7 cells were depicted from these based on their distinctive morphologies. BN-samples were plated at 0.5 cells/well in up to eight 96-well plates, validated, and monitored throughout clonal expansion by automated image-based analysis (Cellavista, Roche). 11–26 single cell-derived subclones were selected per case and expanded. For generation of pilot data, at least 5 subclones were used per patient sample.

Compound screening and treatment

Reference/control cells, parental tumor cells, and subclones were seeded in 96-well plates at 5–13×10^3 cells/cm^2 in triplicates. 24 hours later, drugs were applied as 10× stock-dilutions. Cellular viability determined as ratio of background-subtracted alamarBlue® (Life Technologies) fluorescence intensities of treated and vehicle-control cells. Compounds of the pilot drug screen (Supplementary Table S2) were applied in 6 different concentrations to determine dose-response-levels. 4 days later, cellular viability was compared to vehicle-applications (0.55% DMSO for compounds combined with 50 μM temozolomide (TMZ); 1.5% DMSO for TMZ-treatment alone; 0.5% EtOH for Perifosine and 0.5% DMSO for all other drugs). The "Killer Plates" compound library (Microsource) was applied to GNV019 cells at 1 μM concentrations each, and compared to vehicle-controls (0.01% DMSO) at 5 days after treatment. IC50 evaluation for selected compounds was performed as described (18).

For co-culture, subclones were labeled with green (CellTracker™ Green CMFDA, 5 μM, or Vybrant™ DiO, 1:200) or red fluorescent dyes (CellTracker™ Red CMTPX, 25 μM, or Vybrant™ DiD, 1:200, all Life Technologies) for 30 minutes. Equal quantities of green- and red-labeled cells were seeded on 12-well plates. CL1/2/3/6/7 cells were treated with 10 μM Thioguanine, 2 μM Oridonin, 4 μM Sorafenib, 1 μM Cantharidin or 0.1% DMSO for 5 days. BN035 subclones were treated with 0.4 nM Bortezomib, 8 μM Lonafarnib (+50 μM TMZ), or 0.25% DMSO. BN046 subclones were treated with 3 μM 17-AAG, 10 μM Etoposide (+50 μM TMZ), or 0.15% DMSO for 3 days. Challenged cells were trypsinized for flow cytometry using 15–20×10^3 cells (FACSCalibur Cell Analyzer; BD Biosciences) to determine drug effects.

For subclone selection from parental GNV019 cells, increasing concentrations of Thioguanine or 0.1% DMSO were applied for 5 days, followed by a 4-day growth factor withdrawal-induced differentiation period, before quantifying (giant) multinucleated cells. CL2-*like* cells were selected by single- or repeated-treatment with 4 μM Sorafenib for 5 days. For subclone selection from BN035 and BN046 parental cells, drugs were applied in

two three-day cycles at concentrations indicated (Supplementary Figs. S5B, S6B). Sequential treatment (5+5 days for all) of GNV019 cells (Fig. 6) was either conducted with 10 μM Thioguanine / 0.1% DMSO (1st line) followed by 20 μM Perifosine, 1.5 μM SAHA (+ 50 μM TMZ), 3 μM Sunitinib, 0.5 nM Bortezomib, 100 nM Dasatinib or 0.12% DMSO (2nd line). The alternative course included 4 μM Sorafenib / 0.02% DMSO (1st line) followed by 1 μM Cantharidin, 20 μM Imatinib, 0.5 μM Etoposide (+50 μM TMZ), 0.2% DMSO, 1 mM TMZ, or 1% DMSO (control condition for TMZ alone) (2nd line).

Orthotopic xenograft experiments and animal treatments

Ethical Committees of the Universities of Bonn and Florida approved all animal studies. For engraftment, cells were harvested, counted and resuspended in 0.1% DNase I (Worthington) / PBS (Life Technologies). Cell vitality was confirmed via Trypan blue exclusion. 2 μl encompassing 1×10^5 cells were stereotactically applied to the brains of Fox Chase SCID/beige mice (females, 9–13 weeks old; 1.6 mm anterior, 1.9 mm lateral to the bregma, 1.4 mm deep from the dura; Charles River). In addition to presented data, tumorigenicity and cellular characteristics of GNV019 parental and subclonal cells were confirmed in NMRI nu/nu mice (females, 6–10 weeks old; n=2, each; 2.2 mm anterior, 1.3 mm lateral, 1.7 mm deep; Janvier Labs). Mice were monitored daily and euthanized when signs of neurological impairment or significant weight loss (20% from preoperative weight) was noted. For routine histology, brains were fixed by vascular perfusion (4% formaldehyde). Coronal gradient echo, T2-weighted and fluid-attenuated inversion recovery magnetic resonance imaging (MRI) data were obtained from formaldehyde-fixed whole brains using the core facility of the McKnight Brain Institute (University of Florida) under standard imaging protocols with a 15-mm birdcage coil and 11-T horizontal-bore magnet (Bruker).

In vivo analysis of subclone enrichment commenced at day 42 post orthotopic xenotransplantation of GNV019 parental cells. A 2.5 mg/ml stock solution of Thioguanine (50 mg Thioguanine / 20 ml of 0.02 M NaOH) generated doses of 10 mg/kg per injection and was applied for three consecutive days (21). 100 mg Sorafenib dissolved in 2.5 ml Kolliphor/EtOH (50:50, Sigma Aldrich) to obtain a 4× stock solution was further diluted in ddH$_2$O. 100 mg/kg treatments were conducted on 5/7 days per week (22). Sorafenib-induced population shifts were assessed using DNA from 5/8 animals of the experimental series (2× Kolliphor/EtOH, 3× Sorafenib). 3/8 samples were excluded because sufficient DNA quantity/quality could not be obtained: two samples representing pre-necrotic brain tissue of animals that died over night; one sample failed DNA-extraction.

Immunocytochemistry

Paraformaldehyde-fixed cells and formaldehyde-fixed paraffin-embedded tissues were supplied with primary antibodies against βIII-tubulin (Promega; monoclonal mouse, clone 5G8, 1:1,000), GFAP (DAKO; polyclonal rabbit, #Z0334, 1:600), pan-Cadherin (Thermo Fisher Scientific, polyclonal rabbit; #PA5-19479, 1:200), and α-Tubulin (Sigma Aldrich, monoclonal mouse; clone DM1A; 1:1,000) over night at 4°C. Respective antigens were labeled by incubation with fluorophore-conjugated secondary antibodies (Alexa Fluor® 488 goat anti-mouse IgG 1:800 and Alexa Fluor® 555 goat anti-rabbit IgG 1:500, Life

Technologies) for 1h at room temperature. Cell nuclei were exposed with 2 μg/ml DAPI (Sigma Aldrich) for 10 min. Fluorescence microscopy was performed on a Zeiss Axioskop2 or Axio Imager.Z1 upright microscope. Frequencies of mGCs (*in vivo*) and mGC-like mnCells (*in vitro*) were determined by quantifying mono- vs. multinucleated cells in respective samples using DAPI and α-Tubulin (*in vitro*) or pan-Cadherin (*in vivo*) labeling. Quantification was conducted by averaging the results of at least two investigators (RR, LR, BS) blinded to the experimental conditions.

Molecular Biology

DNA/RNA was isolated using the AllPrep DNA/RNA Mini Kit (Qiagen) following the manufactures instructions. Chromosomal aberrations were analyzed using Illumina's BeadChips (HumanHap550/Human610-Quad). Sample preparation was performed according to Illumina's Infinium protocols. For whole genome gene expression profiling total RNA of biological triplicates was extracted using QIAzol Lysis Reagent (Qiagen) and analyzed using HumanHT-12 v3 expression BeadChips (Illumina). Gene expression and genotyping data were deposited at GEO (Gene Expression Omnibus: accession numbers GSE72927, GSE72732). *TP53* mutation screening was performed according to the direct sequencing protocol of the International Agency for Research on Cancer (Lyon, France). DNA copy numbers were quantified on a ViiA™ 7 Real-Time PCR System (Life Technologies) using SYBR Green. PCR cycling conditions: 95°C for 3 min, followed by 40 cycles at 95°C for 20 s, 60°C for 20 s and 72°C for 30 s. C_t values for target genes on Chr. 1 (*CDKN2C*), Chr. 5 (*SCAMP1, CHD1*), and Chr. 22 (*BID, NF2*) were normalized using C_t values of the Chr. 2 reference genes (*MEMO1* and *ASB3*). Copy number values were calculated using the C_t method on tumor samples and human leukocyte DNA as reference. Gene expression analysis of signature neural stem-like genes was performed as described (18) using 1μg total RNA (for primers, see Supplementary Table S3). Custom multiplex ligation-dependent probe amplification (MLPA) kits (P345-X1 & P346-X1; MRC-Holland) were used to detect copy number alterations in BN035 and BN046 cells. 90 ng DNA from tumor cells or from (two individual) reference human leukocyte DNA were used for each MLPA reaction. Fragment separation was performed on a 3130×l Genetic Analyzer (Applied Biosystems) and MLPA ratios determined using Coffalyser software (MRC-Holland).

Bioinformatics and statistics

Hierarchical clustering, calculation of Pearson correlation coefficients, heatmaps and LogR ratio plots were performed using R-project statistical software (v3.0.2; 23). Molecular subtypes of GNV019 samples classified as 'neural' (according to 24). Cluster dendrograms were created using Euclidean distance and average linkage analysis. All other computations were carried out using GraphPad Prism 6.0f and Microsoft Excel. Where applicable, the two-tailed Student's t test (assuming equal variances), the one-way ANOVA with Tukey correction for multiple comparisons, or the two-way ANOVA with Bonferroni's correction for multiple comparisons were performed for statistical analysis. Standard distribution of data applied for respective tests. Data analysis based on biological triplicates, unless otherwise specified. Unless otherwise indicated, data presented as mean ± SD (levels of

significance: *p <0.05, **p<0.01, ***p<0.001, ****p<0.0001). Cartoons produced using SERVIER Medical Art.

RESULTS

Drug response profiles of tumor subclones reflect intra- and inter-individual tumor heterogeneity

In pilot experiments, we explored single cell-derived (subclonal) cultures from clinical patient samples to display heterogeneity of drug response patterns. Based on reported transcriptome analysis of 430 single cells from 5 glioblastoma patients (25) we expected patterns of strong inter-individual differences and a considerable degree of intra-tumor heterogeneity. In a parallel constellation, we applied short-term expanded primary cell cultures from five glioblastoma patients and, additionally, a total of 33 respective subclones for analysis of differential drug response. All cells were maintained under adherent *in vitro* conditions suited for the expansion of neural stem- and precursor cells (Materials and Methods). 20 clinical trial-grade drugs and compounds (Supplementary Table S2) were used to determine IC50-values, i.e. the individual concentrations that reduced cellular viability by 50% compared to vehicle-control treatments. Hierarchical clustering of data revealed an extent and pattern of heterogeneity comparable to the transcriptome data presented by Patel et al. (25). A strong inter-individual variability was noted as well as substantial intra-individual differences of drug response patterns (Fig. 1). Notably, for each of the five cases, the median drug concentration difference between the most and least resistant subclone revealed a 2-fold intra-individual variability of drug response among all investigated compounds (Supplementary Fig. S1, mean factor= 2.32, range: 1.86–2.92).

Thus, data from our test system indicated considerable variation of drug responsiveness among intra-tumor subclones, adding another level of complexity to the inter-individual differences that are commonly acknowledged in the biology of glioblastoma (24, 26). These pilot data, however, also raised questions. On the one hand related to the overall range of potentially co-existing subclones and intra-individual drug response profiles. On the other hand, it was unclear to what degree the subclones maintain their distinct phenotypic and genetic identities *ex vivo* and whether the determined variability of drug response would impact on the cellular composition of a tumor bulk upon treatment. We prioritized investigation of the latter complex of questions, because the range of intra-tumor response profiles would be irrelevant if significant alterations to the cellular composition of the tumor bulk would not occur.

Morphological, genetic, and functional traits of tumor subclones are preserved *in vitro* and *in vivo*

Previous studies already demonstrated that patient- and disease-specific hallmarks of glioblastoma could be mirrored *ex vivo* for experimental investigation (17, 18, 27). For experimental access to studying consequences of clonal diversity, we selected the case GNV019 that presented with a characteristic morphological trait of heterogeneity: multinucleated giant cells (mGCs). Their presence is not an obligatory finding, but rare mGCs are frequently observed in glioblastoma (16). Histopathology of the patient's tumor

accordingly revealed very few (≈1%) mGCs intermixed with other pleomorphic smaller cell phenotypes (Fig. 2A). Morphological heterogeneity was similarly observed when primary GNV019 cells were isolated and propagated under adherent conditions (Fig. 2B; 20). The cellular expansion rate remained stable, and the disease- and patient-specific gene expression-/ copy number profiles were conserved *in vitro* (Fig. 2C–E; 28, 29). Orthotopic xenotransplantation demonstrated a tumorigenic potential replicating the original tumor's glioblastoma histology, including the presence of intermixed, rare mGCs (2.1±1.1%; n=11; Fig. 2F, G and I). We next investigated sublones (CL1/2/3/6/7) derived from early-passage parental GNV019 cells (Fig. 2H, upper panel). They presented common genomic profiles with only a few differential copy number alterations (Supplementary Fig. S2), and, similar to the parental samples they each classified as 'neural' subtype (24). Notably, however, orthotopic xenotransplantation revealed distinct categories of *in vivo* behavior. CL2 cells were not tumorigenic (n=11/11). The other subclones consistently developed histopathological features of glioblastoma (16), yet their cellular composition varied. CL7-derived tumors appeared 'small cell-enriched': most tumor cells were uniformly small and round, mGCs extremely rare (0.2±0.2%; n=8). By contrast, CL1/3/6-derived tumors presented high mGC frequencies (32.8±9.3%; n=8/7/10; Fig. 2H, lower panel and Fig. 2I).

We concluded that GNV019 disease- and patient-specific characteristics were preserved *ex vivo* and that isolation of tumor subclones enabled functional access to distinguishable morphological characteristics of the parental tumor.

Subclone phenotypes present distinct developmental and genetic traits

We next explored whether the distinct categories of *in vivo* behavior reflected distinct patterns of cellular plasticity, gene expression, and genetic aberrations. *In vitro,* the subclones consistently revealed stem-like developmental potentials, i.e. 5/5 were able to self-renew (Supplementary Fig. S3), and to differentiate into neuronal and glial progeny (Fig. 3A, upper panels). Notably, a pronounced capacity to also generate (giant) multinucleated cells (mnCells) upon spontaneous differentiation *in vitro* that resembled mGCs *in vivo*, was only observed in CL1/3/6 cells matching their developmental potential in xenografts (Fig. 3A, lower panels). Moreover, analysis of signature neural stem-like genes (*FABP7, OTX2, SOX9, BMI1, SOX2, VIM, NOTCH2, VCAM1, NES, NCAM1, SOX8, FGFR4*) indicated distinct expression motives separating non-tumorigenic CL2 cells from tumorigenic mGC-forming CL1/3/6, and from tumorigenic 'small cell-enriching' CL7 cells (Supplementary Fig. S4). Unsupervised clustering of correlation data from genome-wide gene expression and in-depth genotype analysis further confirmed the specific hierarchic alignment of GNV019 subclones (Fig. 3B).

In synthesis, findings indicated consistently distinct morphological, developmental, and genetic traits of the investigated GNV019 subclones *in vitro* and *in vivo,* serving as an ideal basis to reveal functional consequences of intra-tumor heterogeneity.

Distinct pharmacological response patterns enable selection of subclones by *in vitro* drug challenge

The specific alignment of CL1/3/6, CL2, and CL7 – as determined in the functional and molecular classification experiments above, corresponded directly to the drug response profiles of GNV019-derived subclones of our pilot data (Fig. 1). This encouraged further investigation toward pharmacological targeting of distinct subclones. To broaden the approach and for experimental validation, we additionally applied a commercial library comprising 160 synthetic/natural compounds, previously used for identification of new drug candidates in glioblastoma (18). Hierarchical clustering of the respective cellular viability data further confirmed the specific alignment of CL1/3/6, CL2, and CL7 (Fig. 4A).

Together, data suggested that the five investigated GNV019 subclones represented three independent intra-tumor cell hierarchies separating co-existing precursor cells and their descendants by functional, phenotypic and genetic traits. We hypothesized that these hierarchies needed to be considered as functionally distinct intra-tumor cell populations with independent drug resistance profiles. Based on this assumption and the noted stability of subclones *ex vivo*, we opted for discriminative investigation and modeling of intra-tumor population dynamics using GNV019 cells as an experimental system. The approach was initiated by determining the most suitable drugs for pharmacological hierarchy selection, chosen from both sets of compound screening data (Fig. 4B). Subsequent pharmacodynamic analysis established drug concentrations with most pronounced effects. The highest differential level of intrinsic drug resistance was defined at 10 μM Thioguanine (synthetic guanosine analogue antimetabolite, inhibits nucleic acid synthesis) for CL1/3/6 and at 2 μM Oridonin (mechanism of action not yet fully understood) for CL7 cells. CL2 cells could be discriminated from all others by their sensitivity to 1 μM Cantharidin (PP2A-Inhibitor) and by their resistance to 4 μM Sorafenib (multi kinase inhibitor, see Supplementary Table S2) (Fig. 4C). To test the drugs' applicability for pharmacological selection, defined mixtures of fluorescently pre-labeled subclones were exposed in co-culture to a single drug dose and their respective population shifts were evaluated by flow cytometry five days later (Fig. 4D and E). Comparison with vehicle-controls confirmed the predicted targeting of distinct subclones/hierarchies. The resulting mean population shifts were determined at 20±3% in response to *in vitro* drug challenge (Fig. 4F).

Intra-tumoral, treatment-related population dynamics can be predicted *in vitro*

The aforementioned, reductionist co-culture experiments suggested that the ratios of intra-tumoral subclone fractions could be selectively modulated depending on the choice of drug used for pharmacological challenge. In a next series of experiments we aimed to show that this could be applied to the more complex setting of parental GNV019 cells.

In a first approach, parental cells were considered as a polyclonal collection of precursors either responsible for (e.g. Thioguanine-resistant CL1/3/6-*like* cells) or incapable of mGC/mnCell-generation (e.g. Thioguanine-sensitive CL2/7-*like* cells) (Fig. 5A). The morphological trait of mGC/mnCell-generation was used as a read-out parameter to quantify the extent of pharmacological selection. Application of Thioguanine to GNV019 parental cells and subsequent differentiation *in vitro* indeed yielded up to five-fold concentration-

dependent increases of mnCell fractions (Fig. 5B). The corresponding increases correlated with differential viability effects recorded at pharmacodynamic investigation of CL1/3/6 and parental cells (Fig. 5C and D, compare Fig. 4C). In a control setting, we confirmed that Thioguanine alone did not induce the mnCell-phenotype, as its application did not alter the capability of CL2 or CL7 cells to develop the phenotype *in vitro* (Fig. 5E). We concluded that – as predicted, Thioguanine selectively enriched CL1/3/6-*like* cells from the GNV019 parental cells. A second approach based on the presence of a distinctive, 36-megabase-deletion in CL2 cells on chromosome 5q (Fig. 5F). Used as a read-out parameter, a decreased abundance of this chromosomal region would indicate an increased fraction of CL2-*like* cells within the GNV019 parental cells (Fig. 5G). The extent of pharmacological selection was then determined by quantifying copy numbers of genes within the CL2-specific deletion. As predicted, Sorafenib exposure led to dose-dependent copy number decreases indicating an enrichment of CL2-*like* cells from GNV019 parental cells (Fig. 5H, compare Fig. 4C).

These data implied that pharmacological profiling of subclones could blueprint post-hoc identification of individual cell hierarchies in a heterogeneous parental tumor sample. To validate whether this insight could be applied to other glioblastoma specimens, we investigated 14 additional subclones from two more clinical samples of our pilot data set (Fig. 1) adopting the experimental course established on GNV019 cells. Briefly, BN035- and BN046-subclones underwent MLPA analysis for identification of specific genetic marks (Materials and Methods), selection of subclone-specific drugs from pharmacological profiles, respective validation in co-culture, and successful tracking of predicted subclone-enrichment in parental tumor samples (Supplementary Figs. S5 and S6). The consistency of experimental results from all three investigated clinical samples led us conclude that intra-tumoral, treatment-related cellular population dynamics is predictable, based on discriminative investigation of drug responses under controlled *in vitro* conditions.

Intra-tumoral, treatment-related population dynamics can be predicted *in vivo*

Next, orthotopic xenotransplantation validated predictability of drug-induced polyclonal dynamics *in vivo*. Treatments of animals engrafted with 10^5 GNV019 parental cells commenced at day 42, when intracerebral glioblastoma characteristics had already developed (compare Fig. 2F and G). Intraperitoneal (i.p.) vehicle injections yielded a median overall survival (mOS) of 60.5 days (n=3, each; Fig. 5I).

The established morphological/genetic read-out parameters were then used to verify Thioguanine/Sorafenib-induced enrichment of distinct hierarchies, i.e. CL1/3/6-*like* or CL2-*like* cells. Both drugs indeed induced the predicted population shifts, independent of their influence on mOS. Thioguanine-applications were limited to three injections due to potential myelotoxicity (n=6 animals; i.p.; 21) and did not extend the mOS of engrafted animals (Fig. 5I). Nevertheless, a significant 2.8-fold increase of mGCs indicated a treatment-related population shift as predicted (p=0.0149; Fig. 5J). In the parallel experiment, Sorafenib applications (n=5 animals; i.p., dose acc. to 22) extended the mOS significantly to 74 days (p=0.0042) (Fig. 5I). Micro-dissected tumor tissue from these animals then provided evidence for an increasing population size of CL2-*like* cells, as predicted. Quantifying copy

numbers of genes in the CL2-specific region of deletion on chromosome 5q revealed a significant decrease from 2.03±0.05 (vehicle) to 1.83±0.06 (Sorafenib) (p=0.029, Fig. 5K).

Implications of predictable population dynamics for 2nd line treatment strategies

In a last series of experiments, we investigated whether information from *ex vivo* pharmacological profiling and prediction of subclone enrichment could be applied to the design of rational drug combinations. We hypothesized that one drug could be used in a first line setting to drive the heterogeneous parental tumor bulk towards enrichment of particular subclones/hierarchies with distinct sensitivities to a choice of 2nd line drugs. The hypothesis was tested in two settings on GNV019 parental cells, implementing pharmacological profiles as planning tools (Fig. 6A,C). In setting one, we observed enrichment of CL1/3/6-*like* cells with Thioguanine rendering the parental tumor bulk significantly more vulnerable to Perifosine, SAHA+TMZ or Sunitinib, which were predicted particularly effective on CL1/3/6 cells by the initial profiling. By contrast, drugs with minor inhibitory effects on CL1/3/6 cells in the initial profiling, e.g. Bortezomib and Dasatinib, showed a less pronounced effect on bulk tumor cells secondary to Thioguanine application (Fig. 6A,B). In setting two, enrichment of CL2-*like* cells with Sorafenib required Cantharidin for more effective 2nd line inhibition. As predicted from the CL2 profiling, Imatinib, Etoposide+TMZ, and TMZ were less appropriate 2nd line combinations for Sorafinib (Fig. 6C,D). In a control arm for both sets of experiments, we could furthermore show that these effects were exclusive to the parental bulk of tumor cells (Supplementary Fig. S7).

We conclude that *ex vivo* drug profiling of tumor subclones can facilitate predictions on treatment-related population dynamics and that rational drug combinations for sequential application in glioblastoma can be identified.

DISCUSSION

Our study considers glioblastoma as polyclonal collection of potent cellular hierarchies – at least at clinical manifestation of disease. The concept combines classic stochastic and cancer stem cell models (2, 12) implying that subclones with distinct intrinsic resistance profiles co-exist in tumor specimens. While poor or short-lasting therapy responses still occur in most glioblastoma patients, we here show the applicability of discriminative *ex vivo* drug profiling of subclones from clinical samples. A previously unrecognized feasibility is revealed enabling predictions on intra-tumoral drug response and the resulting population shifts in bulk tumor samples. This note has important implications, particularly in light of the additional finding that pharmacological profiles could serve as a valuable asset for defining appropriate drug combinations for individualized sequential application.

The roots of our work are classic cell culture studies describing intra-tumoral diversity of karyotypes, phenotypes, and pharmacological responses in human glioma (30–32), recently revisited by investigating patterns of receptor tyrosine kinase amplifications and their respective functional dependence *in vitro* (33). Taking advantage of stem-/precursor culture conditions that enable maintenance of phenotypic and genetic properties, we demonstrate that isolated subclones are amenable for profiling and for predictions on drug-related intra-tumoral dynamics. The importance of investigating alterations to the cellular composition of

solid cancers before and after treatment is being increasingly revealed (e.g. 34, 35). Drug-related enrichments of primary resistant cell types may even include minority cellular hierarchies of the original tumor (36, 37). This could be recapitulated in our model by the significant drug-related enrichment of CL1/3/6-*like* or CL2-*like* GNV019 hierarchies. We observed the effect even occurring independent of a survival benefit in xenografts. A logical next step for future follow-up would be a study on matched clinical samples obtained before and after treatment to provide unequivocal evidence that predictable drug-related clonal selection occurs in glioblastoma patients. We already know that successful eradication of targeted neoplastic cells cannot prevent the cells that were not targeted to develop fatal relapse (e.g. 38). Predictable population dynamics could serve as a valuable asset on these grounds for defining appropriate secondary lines of treatment. It might even be essential, because secondary surgery cannot always be performed in glioblastoma and current practice of care frequently considers re-challenge of first-line pharmacotherapy for treating relapsed disease (39).

It needs to be emphasized, however, that our approach focused on the feature of primary/intrinsic resistance. Further investigation may be directed, e.g., towards acquired drug resistance and potential subclone interactions, as well as towards environmental and immunological cues for a more comprehensive view (12, 40–42). Some of these factors, in addition to animal model-inherent obstacles, including potentially suboptimal drug dosage / pharmacokinetics / distribution, might already explain the lower efficacy of *in vivo* vs. *in vitro* subclone enrichment observed in our study. Another restriction may apply to conditions for derivation and expansion of clinical samples. While our work shows how cellular heterogeneity can be captured and how cellular identity can remain stable under adherent conditions, it is known that any setting of primary cell culture may inflict selection bias on patient tissue and cells (e.g., 43). Thus, even though we present data on drug-mediated enrichment of 19 subclones from three clinical specimens, sufficient data is not available for a statistically valid extrapolation of clonal diversity. This could be addressed in future, e.g. by introducing artificial DNA barcodes to the entire population facilitating quantification of individual subclones in the tumor bulk (44).

Our study furthermore provides tools for individualizing medicine, e.g. specifying how subclone drug profiles could help to foster translational studies and more personalized approaches addressing the functional consequences of intra-tumor heterogeneity (see Supplementary Fig. S8). In our study, ternary plots serve as schematic representations of subclone drug profiles. They correlate the degree of drug sensitivity among co-existing tumor cell hierarchies in a two-dimensional plot. Applied as a planning tool, suited pairs of drugs can be identified that drive the heterogeneous parental tumor bulk towards enrichment of a particular subclone/hierarchy during first line application and that aim for depletion of this hierarchy in the 2nd line approach. Granted that future developments in clinical medicine will improve upon many of the technical aspects of our work, e.g. toward a more complete mirroring of subclone heterogeneity from clinical specimens, our approach could provide the rationale for personalizing sequential therapy in glioblastoma. For basic sciences, the approach could enable investigation of potential relationships between drug-specific mechanisms of actions, differential drug sensitivities, and the various molecular signatures

provided by intra-tumor hierarchies. Also, pre-clinical limitations, e.g. inflicted by combinatorial vs. sequential drug application could be studied in a reductionist setting.

Taken together, our observations support accumulating evidence from the study of many malignant types of cancer and the notion that population-level methods could underestimate clinically relevant information (3–5, 14, 36, 45). Pharmacological predictions on tumor dynamics would smoothly integrate into the intense ongoing search for new and alternative pharmacotherapy options, particularly needed in the setting of defining individualized 2nd line treatment strategies. Combined with advanced genetic diagnostics and driven by the high medical need in glioblastoma, this strategy might become an essential tool for precision medicine and clinical trial design (9).

Supplementary Material

Refer to Web version on PubMed Central for supplementary material.

Acknowledgments

REFERENCES

1. Nowell PC. The clonal evolution of tumor cell populations. Science. 1976; 194:23–28. [PubMed: 959840]

2. Hanahan D, Weinberg RA. Hallmarks of cancer: the next generation. Cell. 2011; 144:646–674. [PubMed: 21376230]

3. Navin N, Kendall J, Troge J, Andrews P, Rodgers L, McIndoo J, et al. Tumour evolution inferred by single-cell sequencing. Nature. 2011; 472:90–94. [PubMed: 21399628]

4. Snuderl M, Fazlollahi L, Le LP, Nitta M, Zhelyazkova BH, Davidson CJ, et al. Mosaic amplification of multiple receptor tyrosine kinase genes in glioblastoma. Cancer Cell. 2011; 20:810–817. [PubMed: 22137795]

5. Gerlinger M, Rowan AJ, Horswell S, Larkin J, Endesfelder D, Gronroos E, et al. Intratumor heterogeneity and branched evolution revealed by multiregion sequencing. N Engl J Med. 2012; 366:883–892. [PubMed: 22397650]

6. Maley CC, Galipeau PC, Finley JC, Wongsurawat VJ, Li X, Sanchez CA, et al. Genetic clonal diversity predicts progression to esophageal adenocarcinoma. Nat Genet. 2006; 38:468–473. [PubMed: 16565718]

7. Yap TA, Gerlinger M, Futreal PA, Pusztai L, Swanton C. Intratumor heterogeneity: seeing the wood for the trees. Sci Transl Med. 2012; 4:127ps10.

8. Mroz EA, Tward AD, Pickering CR, Myers JN, Ferris RL, Rocco JW. High intratumor genetic heterogeneity is related to worse outcome in patients with head and neck squamous cell carcinoma. Cancer. 2013; 119:3034–3042. [PubMed: 23696076]

9. Bedard PL, Hansen AR, Ratain MJ, Siu LL. Tumour heterogeneity in the clinic. Nature. 2013; 501:355–364. [PubMed: 24048068]

10. Ashworth A, Lord CJ, Reis-Filho JS. Genetic interactions in cancer progression and treatment. Cell. 2011; 145:30–38. [PubMed: 21458666]

11. Westphal M, Lamszus K. The neurobiology of gliomas: from cell biology to the development of therapeutic approaches. Nat Rev Neurosci. 2011; 12:495–508. [PubMed: 21811295]

12. Valent P, Bonnet D, De Maria R, Lapidot T, Copland M, Melo JV, et al. Cancer stem cell definitions and terminology: the devil is in the details. Nature reviews Cancer. 2012; 12:767–775.

13. Meacham CE, Morrison SJ. Tumour heterogeneity and cancer cell plasticity. Nature. 2013; 501:328–337. [PubMed: 24048065]

14. Meyer M, Reimand J, Lan X, Head R, Zhu X, Kushida M, et al. Single cell-derived clonal analysis of human glioblastoma links functional and genomic heterogeneity. Proceedings of the National Academy of Sciences of the United States of America. 2015; 112:851–856. [PubMed: 25561528]

15. Louis DN, Ohgaki H, Wiestler OD, Cavenee WK, Burger PC, Jouvet A, et al. The 2007 WHO classification of tumours of the central nervous system. Acta Neuropathol. 2007; 114:97–109. [PubMed: 17618441]

16. Louis, DN.; Ohgaki, H.; Wiestler, OD.; Cavenee, WK. WHO Classification of Tumours of the Central Nervous System. Geneva: World Health Organization; 2007.

17. Glas M, Rath BH, Simon M, Reinartz R, Schramme A, Trageser D, et al. Residual tumor cells are unique cellular targets in glioblastoma. Ann Neurol. 2010; 68:264–269. [PubMed: 20695020]

18. Wieland A, Trageser D, Gogolok S, Reinartz R, Hofer H, Keller M, et al. Anticancer effects of niclosamide in human glioblastoma. Clin Cancer Res. 2013; 19:4124–4136. [PubMed: 23908450]

19. Koch P, Opitz T, Steinbeck JA, Ladewig J, Brustle O. A rosette-type, self-renewing human ES cell-derived neural stem cell with potential for in vitro instruction and synaptic integration. Proceedings of the National Academy of Sciences of the United States of America. 2009; 106:3225–3230. [PubMed: 19218428]

20. Scheffler B, Walton NM, Lin DD, Goetz AK, Enikolopov G, Roper SN, et al. Phenotypic and functional characterization of adult brain neuropoiesis. Proceedings of the National Academy of Sciences of the United States of America. 2005; 102:9353–9358. [PubMed: 15961540]

21. Adams DH, Bowman BM. The chemotherapy of established sarcoma 180 and adenocarcinoma 755 tumors with 6-Thioguanine. Cancer Res. 1963; 23:883–889. [PubMed: 14079152]

22. Siegelin MD, Raskett CM, Gilbert CA, Ross AH, Altieri DC. Sorafenib exerts anti-glioma activity in vitro and in vivo. Neurosci Lett. 2010; 478:165–170. [PubMed: 20470863]

23. R Core Team. R: A language and environment for statistical computing. Vienna: R Foundation for Statistical Computing; 2013.

24. Verhaak RG, Hoadley KA, Purdom E, Wang V, Qi Y, Wilkerson MD, et al. Integrated genomic analysis identifies clinically relevant subtypes of glioblastoma characterized by abnormalities in PDGFRA, IDH1, EGFR, and NF1. Cancer Cell. 2010; 17:98–110. [PubMed: 20129251]

25. Patel AP, Tirosh I, Trombetta JJ, Shalek AK, Gillespie SM, Wakimoto H, et al. Single-cell RNA-seq highlights intratumoral heterogeneity in primary glioblastoma. Science. 2014; 344:1396–1401. [PubMed: 24925914]

26. Hegi ME, Diserens AC, Gorlia T, Hamou MF, de Tribolet N, Weller M, et al. MGMT gene silencing and benefit from temozolomide in glioblastoma. N Engl J Med. 2005; 352:997–1003. [PubMed: 15758010]

27. Pollard SM, Yoshikawa K, Clarke ID, Danovi D, Stricker S, Russell R, et al. Glioma stem cell lines expanded in adherent culture have tumor-specific phenotypes and are suitable for chemical and genetic screens. Cell Stem Cell. 2009; 4:568–580. [PubMed: 19497285]

28. Beroukhim R, Getz G, Nghiemphu L, Barretina J, Hsueh T, Linhart D, et al. Assessing the significance of chromosomal aberrations in cancer: methodology and application to glioma.

Proceedings of the National Academy of Sciences of the United States of America. 2007; 104:20007–20012. [PubMed: 18077431]

29. Cancer Genome Atlas Research Network. Comprehensive genomic characterization defines human glioblastoma genes and core pathways. Nature. 2008; 455:1061–1068. [PubMed: 18772890]

30. Shapiro JR, Yung WK, Shapiro WR. Isolation, karyotype, and clonal growth of heterogeneous subpopulations of human malignant gliomas. Cancer Res. 1981; 41:2349–2359. [PubMed: 7016313]

31. Wikstrand CJ, Bigner SH, Bigner DD. Demonstration of complex antigenic heterogeneity in a human glioma cell line and eight derived clones by specific monoclonal antibodies. Cancer Res. 1983; 43:3327–3334. [PubMed: 6303581]

32. Yung WK, Shapiro JR, Shapiro WR. Heterogeneous chemosensitivities of subpopulations of human glioma cells in culture. Cancer Res. 1982; 42:992–998. [PubMed: 7199383]

33. Szerlip NJ, Pedraza A, Chakravarty D, Azim M, McGuire J, Fang Y, et al. Intratumoral heterogeneity of receptor tyrosine kinases EGFR and PDGFRA amplification in glioblastoma defines subpopulations with distinct growth factor response. Proceedings of the National Academy of Sciences of the United States of America. 2012; 109:3041–3046. [PubMed: 22323597]

34. Almendro V, Cheng YK, Randles A, Itzkovitz S, Marusyk A, Ametller E, et al. Inference of tumor evolution during chemotherapy by computational modeling and in situ analysis of genetic and phenotypic cellular diversity. Cell Rep. 2014; 6:514–527. [PubMed: 24462293]

35. Kim J, Lee IH, Cho HJ, Park CK, Jung YS, Kim Y, et al. Spatiotemporal evolution of the primary glioblastoma genome. Cancer Cell. 2015; 28(3):318–328. [PubMed: 26373279]

36. Diaz LA Jr, Williams RT, Wu J, Kinde I, Hecht JR, Berlin J, et al. The molecular evolution of acquired resistance to targeted EGFR blockade in colorectal cancers. Nature. 2012; 486:537–540. [PubMed: 22722843]

37. Kreso A, O'Brien CA, van Galen P, Gan OI, Notta F, Brown AM, et al. Variable clonal repopulation dynamics influence chemotherapy response in colorectal cancer. Science. 2013; 339:543–548. [PubMed: 23239622]

38. Sampson JH, Heimberger AB, Archer GE, Aldape KD, Friedman AH, Friedman HS, et al. Immunologic escape after prolonged progression-free survival with epidermal growth factor receptor variant III peptide vaccination in patients with newly diagnosed glioblastoma. J Clin Oncol. 2010; 28:4722–4729. [PubMed: 20921459]

39. Weller M, Cloughesy T, Perry JR, Wick W. Standards of care for treatment of recurrent glioblastoma--are we there yet? Neuro Oncol. 2013; 15:4–27. [PubMed: 23136223]

40. Marusyk A, Almendro V, Polyak K. Intra-tumour heterogeneity: a looking glass for cancer? Nature reviews Cancer. 2012; 12:323–334. [PubMed: 22513401]

41. Vermeulen L, de Sousa e Melo F, Richel DJ, Medema JP. The developing cancer stem-cell model: clinical challenges and opportunities. Lancet Oncol. 2012; 13:e83–e89. [PubMed: 22300863]

42. Cloughesy TF, Cavenee WK, Mischel PS. Glioblastoma: from molecular pathology to targeted treatment. Annu Rev Pathol. 2014; 9:1–25. [PubMed: 23937436]

43. Reynolds BA, Vescovi AL. Brain cancer stem cells: Think twice before going flat. Cell Stem Cell. 2009; 5(5):466–467. [PubMed: 19896437]

44. Bhang HE, Ruddy DA, Krishnamurthy Radhakrishna V, Caushi JX, Zhao R, Hims MM, et al. Studying clonal dynamics in response to cancer therapy using high-complexity barcoding. Nat Med. 2015; 21(5):440–448. [PubMed: 25849130]

45. Sottoriva A, Spiteri I, Piccirillo SG, Touloumis A, Collins VP, Marioni JC, et al. Intratumor heterogeneity in human glioblastoma reflects cancer evolutionary dynamics. Proceedings of the National Academy of Sciences of the United States of America. 2013; 110:4009–4014. [PubMed: 23412337]

TRANSLATIONAL RELEVANCE

Inevitably recurring tumor growth complicates even most promising pharmacotherapies in glioblastoma. Arguing that co-existing cellular hierarchies contributing to pharmaco-resistance are extractable from clinical samples we here show that phenotypic and genetic stability of intra-tumor subclones enables controlled and discriminative drug profiling *ex vivo*. Our data imply that the respective profiles are directly applicable to predict intra-tumoral treatment-induced clonal population shifts *in vitro* and *in vivo* - and thus to predict the cellular composition of relapsing human cancer tissue at the time of primary diagnosis. Additionally, we show that pharmacological profiles could serve as a valuable asset for defining combinatorial secondary lines of treatment. Further development of this strategy may be key to the understanding of therapeutic failure, and it may become a sophisticated evidence-based planning-tool for personalizing therapy in glioblastoma.
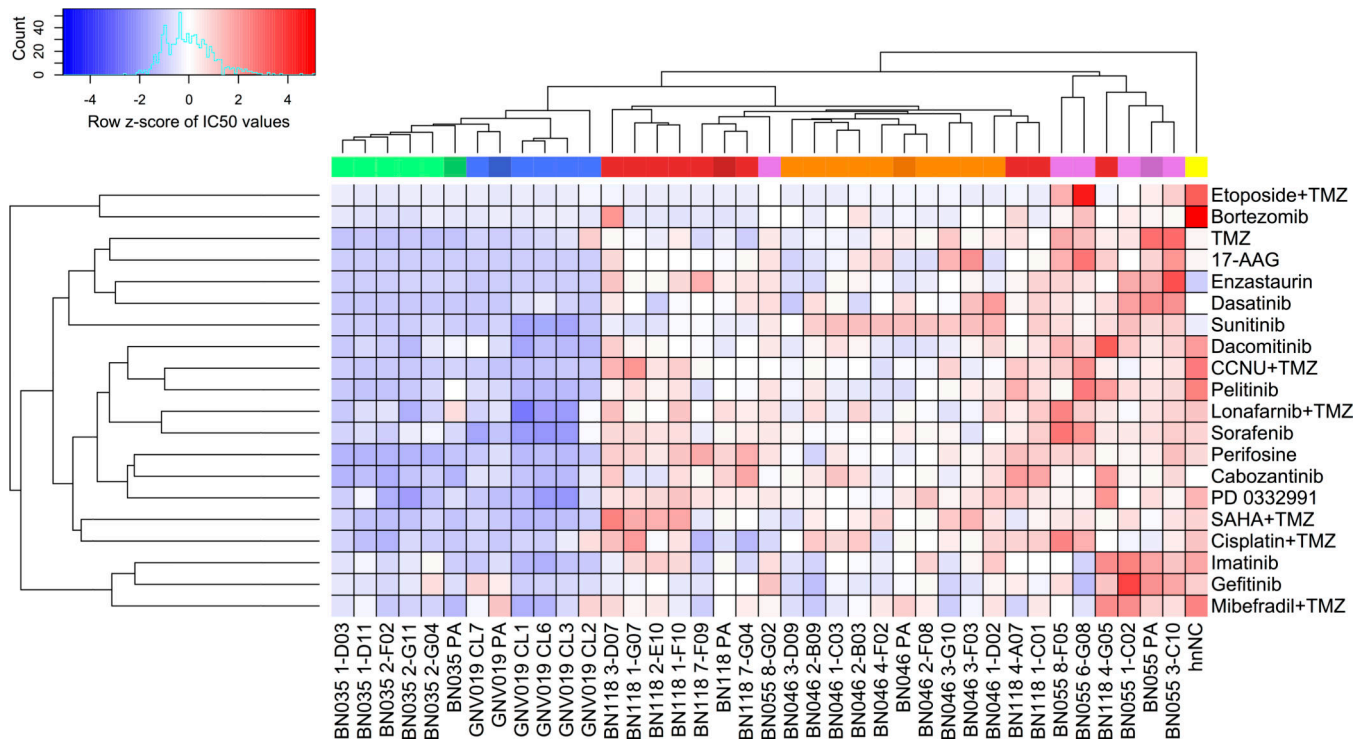
Figure 1.
Pilot data: drug response profiles of tumor subclones reflect intra- and inter-individual tumor heterogeneity. Unsupervised clustering of Z-score transformed IC50 data. Column color code identifies five glioblastoma cases, their respective parental cultures (i.e. one dark shade per color), and their respective subclones (light shades). Data matrix codes reflect low (blue) vs. high (red) IC50 values. Consistency of results was verified by correlating triplicate analysis of two individual library batches (R^2=0.994). hnNCs are human non-malignant brain cells (see Materials and Methods). For individual results and drug/compound details, see Supplementary Fig. S1 and Table S2. Note considerable variability of inter-tumor (29/33 subclones grouped within their patient-specific cluster) and intra-tumor (4/33 subclones even presented as outliers clustering 'trans-individually') drug responses.
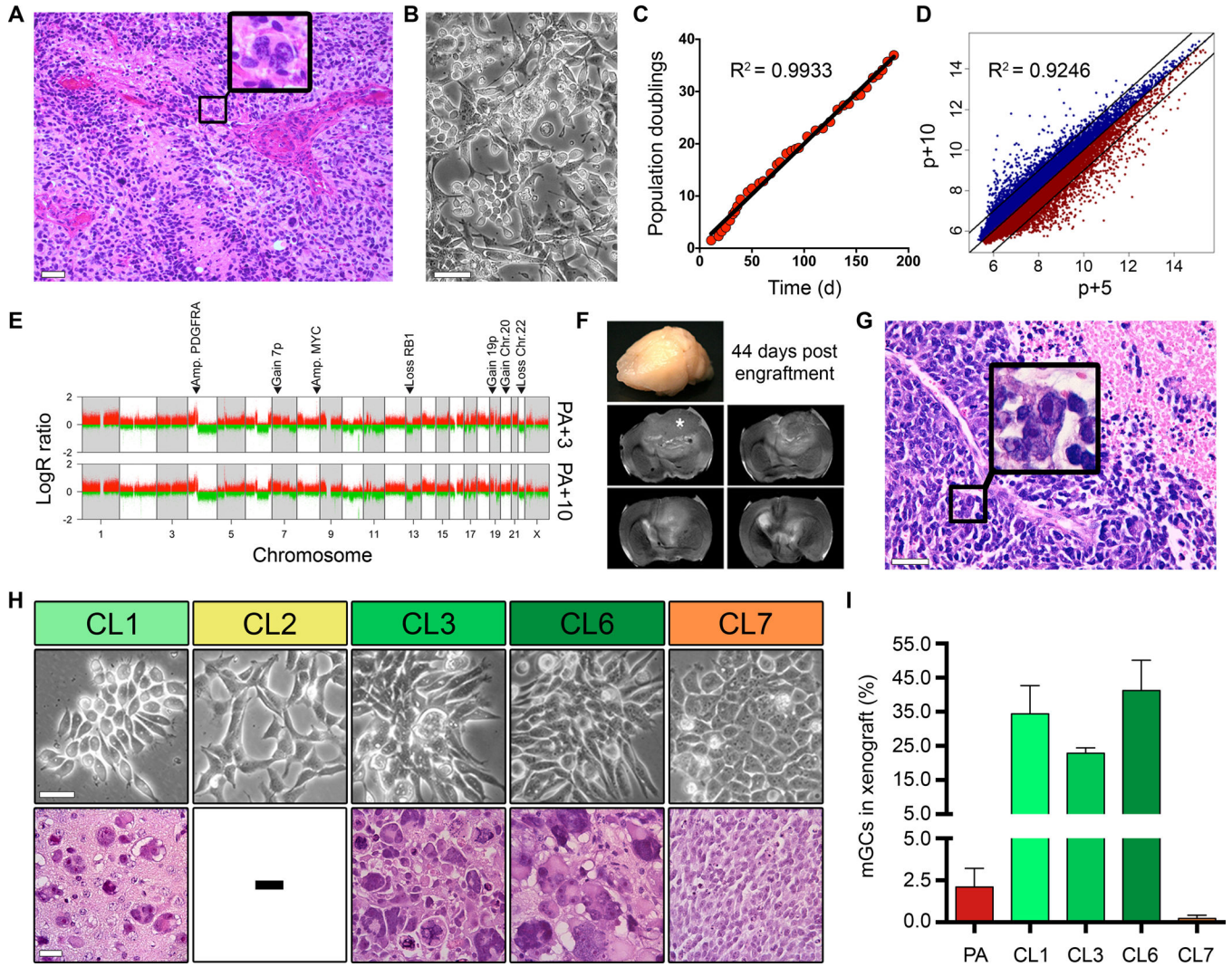
Figure 2.

Morphological, genetic, and functional traits of tumor subclones are preserved *in vitro* and *in vivo*. (A) H&E stained original tissue biopsy (case GNV019) diagnosed as glioblastoma. Typical necrosis, microvascular proliferation, and mitotically active glial cells are present. Note the rare mGCs (example highlighted in box). (B) Phase contrast appearance of GNV019 parental cells, and (C) respective growth kinetics for 35 passages *in vitro*. (D) Scatterplot of log2-transformed whole genome gene expression data from passage 5 and passage 10 GNV019 parental cells revealing high correlation. 96.8% of all expressed genes are found within the 2-fold demarcated area. (E) LogR ratio plots illustrating glioblastoma-typic aberrations (28, 29) from passage 3 vs. passage 10 GNV019 parental cells. Note the overlap. (F) Serial coronal T2-weighted MRI of an *ex vivo* recipient SCID-beige mouse whole brain demonstrating development of a large T2-intermediate mass infiltrating left frontal cortex and subjacent basal ganglia 44 days after xenografting GNV019 parental cells (asterisk indicates original transplant site). There is herniation and midline shift from substantial mass effect (G) Microscopic appearance of the respective xenograft (H&E, tissue section). Note the similarity of pathology to the original patient specimen (Fig. 2A). One of

the rare mGCs is exposed (box). (H) Subclones derived from GNV019 parental cells at passage 5. Upper panel depicts their phase contrast appearance *in vitro*. Lower panel: H&E stains expose distinct xenograft morphologies. CL2 cells were not tumorigenic. (I) Distribution of mGCs in respective xenografts. For quantification, a mean of 10,145 cells were counted in 3–10 random 40× fields per case. PA=GNV019 parental cells. Scale bars: A, 250 μm; B, H 50 μm; G, 100 μm. See also Supplementary Fig. S2.
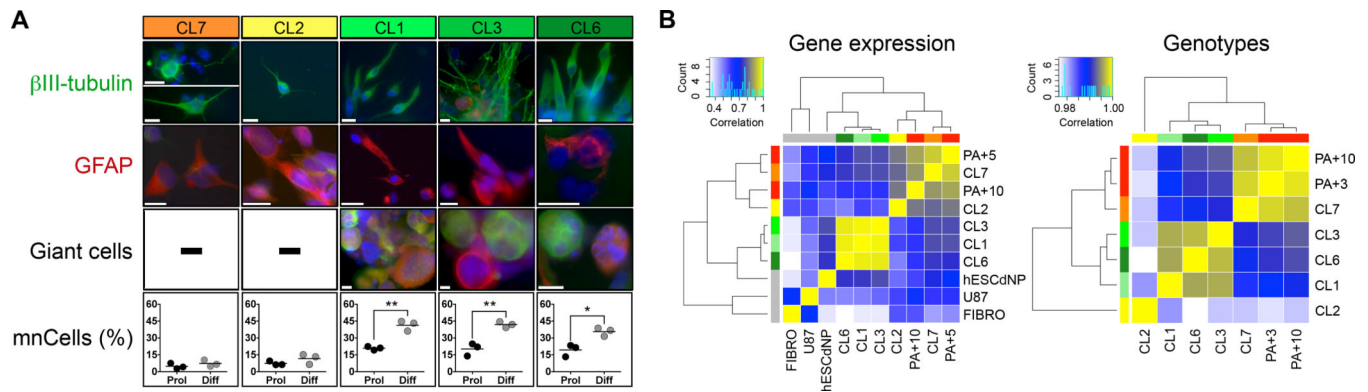
Figure 3.
Subclone phenotypes present distinct developmental and genetic traits. (A) Neurosphere assay (Materials and Methods) testing the differentiation potential of GNV019 subclones *in vitro.* Secondary neurospheres derived from individual subclones were plated and analyzed 10–26 days after growth factor withdrawal. Spontaneous differentiation always yielded neuronal (βIII-tubulin[+]) and glial (GFAP[+]) progeny. Quantification of (giant) multinucleated cells (mnCells) based on counting 1,158±172 cells per condition, i.e. proliferative (Prol) vs. 4-day growth factor withdrawal (Diff) *in vitro* (n=3 independent experiments, each). (B) Correlation heatmaps of gene expression and genotype data. Left: To focus on transcriptional differences the 1,000 most variably expressed genes were identified from genome wide gene expression datasets of GNV019 parental cells and subclones / hESCdNPs / U87 and human fibroblasts (Materials and Methods). Expression values of these genes were correlated between all samples, and respective Pearson correlation coefficients from every single correlation analysis were illustrated as heatmap and clustered using Euclidean distance and average linkage analysis. Right: 550,316 B allele frequency values from the SNP array dataset (Materials and Methods) were correlated between all case GNV019 samples. Pearson correlation values from every single correlation analysis were then illustrated as heatmap and clustered using Euclidean distance and average linkage analysis. Note the high correlation values. Color keys indicate Pearson correlation values. Note the consistent alignment of tumor subclones. PA+3/5/10, GNV019 parental cells at the respective cell culture passage. FIBRO, human fibroblasts; U87, glioma cell line; hESCdNP, non-cancerous human ES cell-derived neural precursor cells (19). Scale bars: A, 20 μm. Significance levels: *p<0.05; **p<0.01. See also Supplementary Fig. S4.
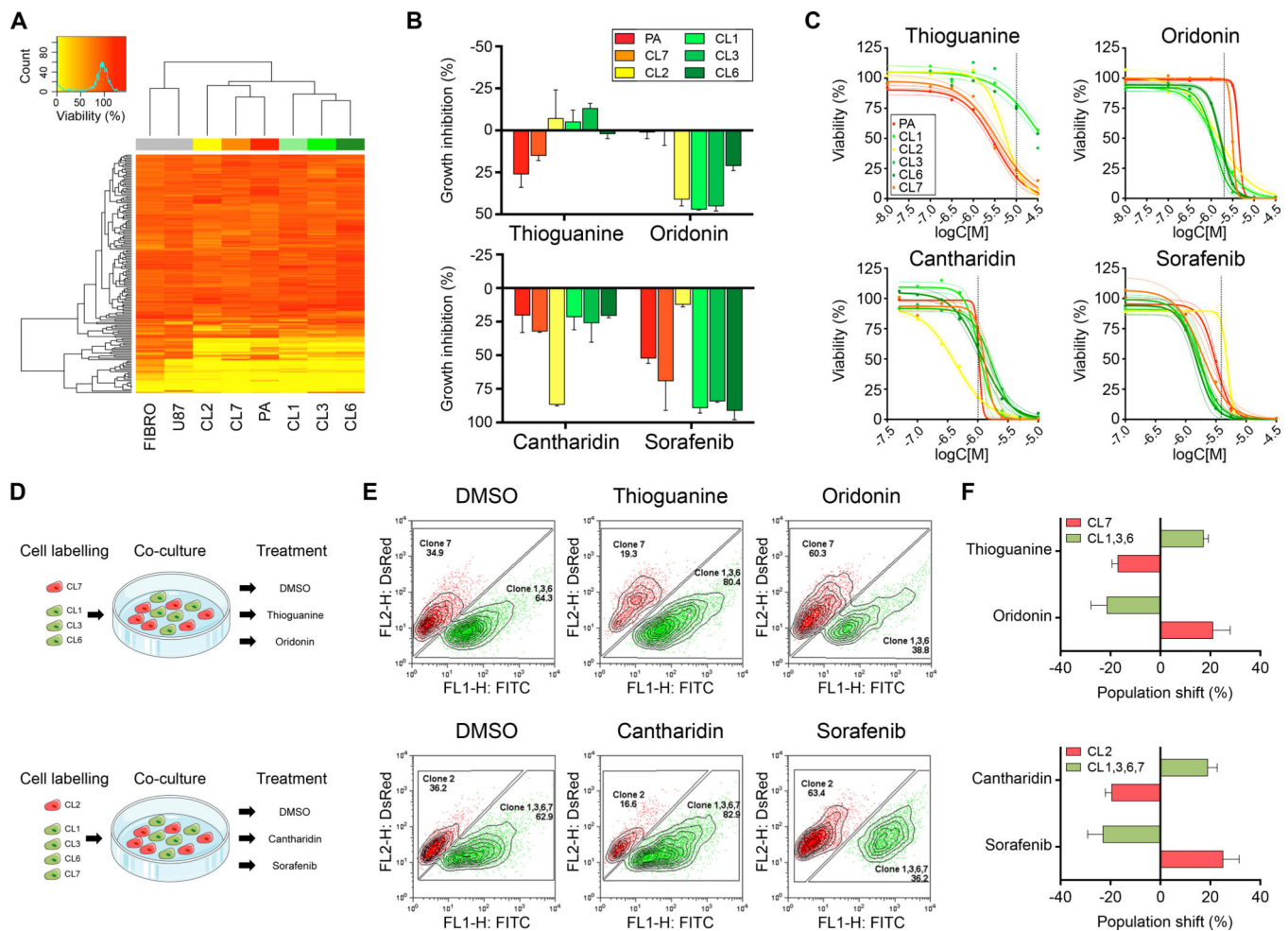
Figure 4.
Distinct pharmacological response patterns enable selection of subclones by *in vitro* drug challenge. (A) The 'Killer Plates' collection was applied (1 μM, each) to record pharmacological responses of GNV019 cell samples. The heatmap illustrates unsupervised clustered viability values (FIBRO, human fibroblasts; U87, glioma cell line; PA, GNV019 parental cells). (B) Subset of data from Fig. 4A, including Sorafenib (applied at 3.16 μM) from set of pilot screening data, suggesting candidate compounds for pharmacological selection of GNV019 subclones. Growth inhibition determined from viability analysis. (C) Dose response curves of candidate compounds. Colored dashed lines indicate the 95% confidence interval of the non-linear regression curve. Dashed vertical lines indicate drug concentrations chosen for further pharmacological selection studies. (D) Experimental co-culture paradigm. For each experiment, equal amounts of red vs. green pre-labeled GNV019 subclones were mixed and exposed to the indicated compounds. (E) At 5 days after exposure at least 15,000 co-cultured cells were quantified by FACS analysis. Shown are representative plots indicating drug-induced shifts of population size among pre-labeled subclones in co-culture. (F) Graphs depict the respective population shifts as calculated by subtracting the percentage of the DMSO-treated control cells from the drug-treated cells (n=3 experiments, each).
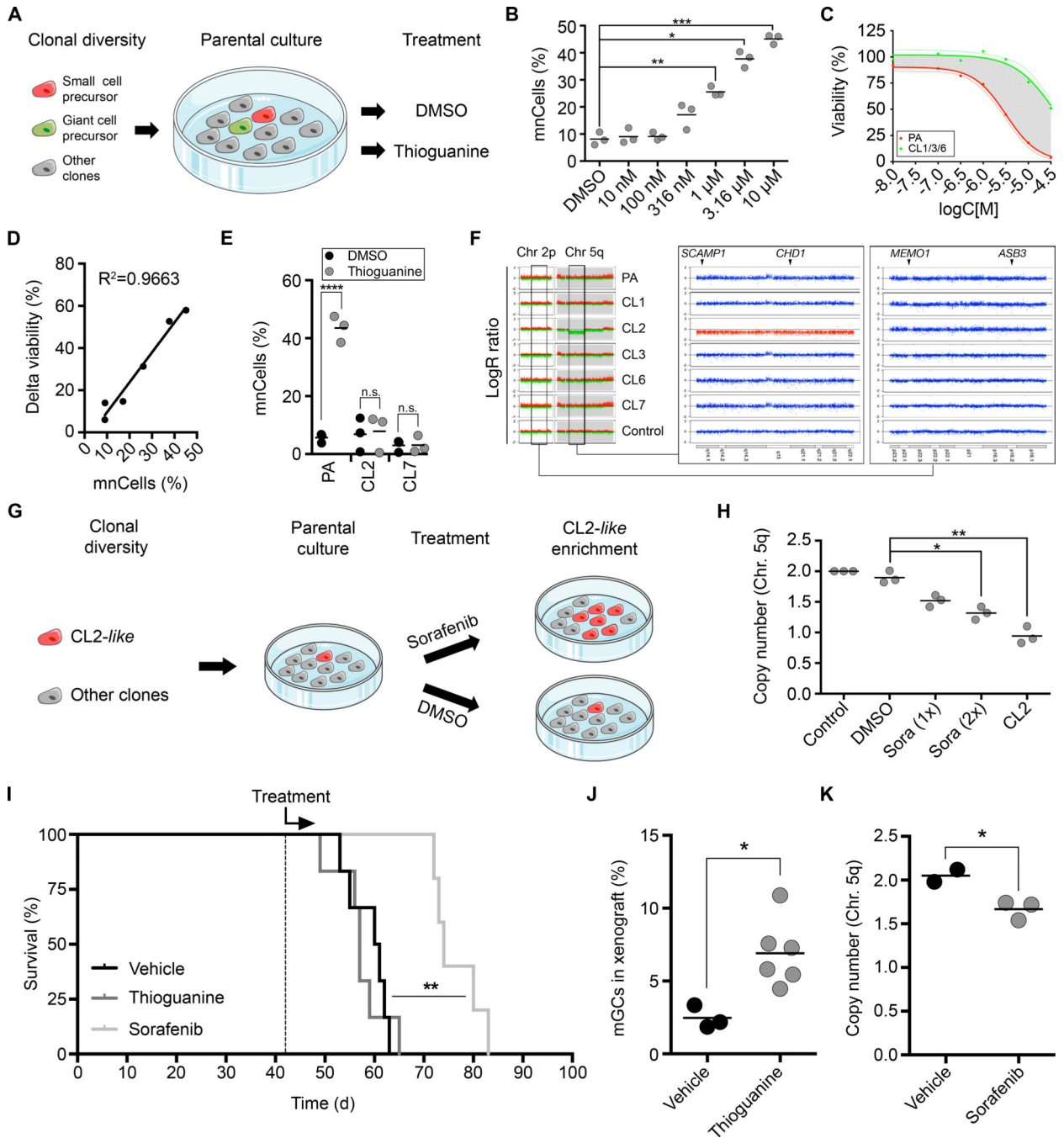
Figure 5.

Intra-tumoral, treatment-related population dynamics can be predicted *in vitro* (A–H) and *in vivo* (I–K). (A) Paradigm using GNV019 parental cells for subclone enrichment experiments. (B) Graph depicts rise of (giant) multinucleated cell (mnCells) frequencies in response to increasing concentrations of Thioguanine (5-day-treatment plus 4-day-differentiation). Quantification based on counting 306±117 cells per condition (n=3 experiments, each). (C) Dose-response-curve on GNV019 parental cells vs. mean values from CL1/3/6 cells. Shaded area highlights difference between both curves (delta viability).

(D) Linear regression analysis correlating mnCell frequencies (from Fig. 5B) with delta viability (from Fig. 5C). (E) Graph showing drug effects on CL2/7 cells vs. GNV019 parental cells. Quantification of mnCells based on counting 674±428 cells per condition (n=3 experiments, each). (F) LogR ratio plot (scale −2/+2) of CL2-specific deletion (middle panel, red: 5q14.1-q22.1). For qRT-PCR DNA copy number analysis primers were designed for intra (*SCAMP1*/*CHD1*) and extra (Chr. 2p23.2-16.1)-deletion genes (*MEMO1*/*ASB3*) as indicated. (G) Paradigm using GNV019 parental cells for subclone enrichment experiments: Sorafenib (4 μM) or DMSO (0.02%) was applied for 5 days (1–2 cycles) followed by DNA isolation for copy number quantification. (H) Graph depicts respective copy number quantification data, normalized using normal human leukocyte DNA (n=3 experiments, each). (I) Kaplan-Meier graph illustrating initiation of treatment (dashed line) and survival times of animals xenotransplanted with GNV019 parental cells. Note, the graph combines survival statistics for NaOH and Kolliphor/EtOH-vehicle controls. Shown level of significance reflects Mantel-Cox test results for Sorafenib- vs. Kolliphor/EtOH-treated animals. (J) Graph depicts blinded quantification of mGCs in vehicle (0.02 M NaOH, n=3) vs. Thioguanine (3×10 mg/kg, n=6)-treated animals sacrificed at the end of the experiment. (K) Graph depicts qRT-PCR DNA copy number analysis conducted in analogy to Fig. 5H. Microdissected tissue derived from animals treated with Sorafenib (100 mg/kg, n=3) was compared with tissue from Kolliphor/EtOH-treated (12.5%/12.5% in ddH2O, n=2) animals. Significance levels: *p<0.05; **p<0.01; ***p<0.001; ****p<0.0001; n.s., not significant.
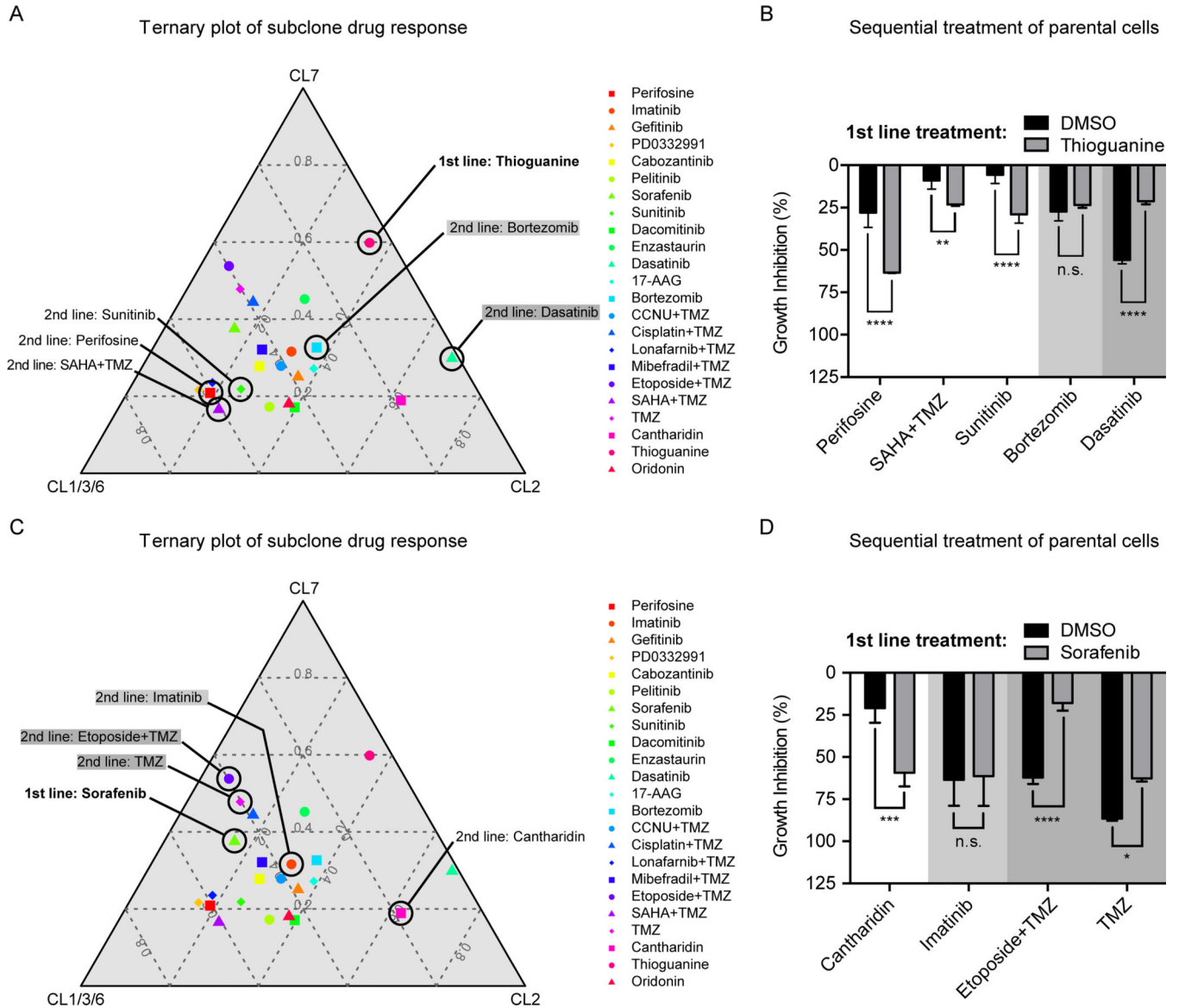
Figure 6.
Implications of predictable population dynamics for 2nd line treatment strategies. (A) Ternary plots visualize the pharmacological profiling data of the three GNV019 hierarchies in a two-dimensional plot (IC50 values, average data for CL1/3/6; comp. Fig. 1, 4C, Supplementary Fig. S1). Every data point represents the positioning of a tested drug in relation to the respective cellular hierarchies. A drug that plots in close proximity to an edge in the graph has a strong inhibitory effect on the respective hierarchy and little effects on the others. Increasing distance from a corner implies decreasing sensitivity of the drug toward the respective hierarchy. For the first line setting of Thioguanine-based enrichment of CL1/3/6-*like* cells, 2nd line drugs were chosen as indicated in the plot: Sunitinib, Perifosine, and SAHA+TMZ plotted close to the CL1/3/6 hierarchy, thus predicted highly effective sequential partners. Bortezomib (light gray) and Dasatinib (dark gray) were predicted less effective. (B) Investigations on GNV019 parental cells: graph representing data from

sequential application of Thioguanine/DMSO followed by the chosen drugs from (Fig. 6A). Note the high consistency of predictions on effectiveness of 2nd line drug applications. (C) For the first line setting of Sorafenib-based enrichment of CL2-*like* cells, 2nd line drugs were chosen as indicated in the plot: Cantharidin plotted close to the CL2 hierarchy, thus predicted a highly effective sequential partner. Imatinib (light gray) and TMZ / Etoposide +TMZ (dark gray) were predicted less effective. (D) Investigations on GNV019 parental cells: graph representing data from sequential application of Sorafenib/DMSO followed by the chosen drugs from (Fig. 6C). Note the high consistency of predictions on effectiveness of 2nd line drug applications. Experiments performed in triplicates. Significance levels: *$p<0.05$; **$p<0.01$; ***$p<0.001$; ****$p<0.0001$; n.s., not significant.